J. Chem. Sci., Vol. 121, No. 5, September 2009, pp. 745–756.

Structure transitions between copper-sulphate and copper-chloride UPD phases on Au(111)†

ILYA V POBELOV[1,2,*], GÁBOR NAGY[2,3] and THOMAS WANDLOWSKI[1,2,*]

[1]Department of Chemistry and Biochemistry, University of Bern, Freiestrasse 3, CH-3012 Bern, Switzerland

[2]Institute of Bio- and Nanosystems IBN 3 and Center of Nanoelectronic Systems for Informational Technology, Research Center Jülich, D-52425 Jülich, Germany

[3]European Commission, Place Madou 1, 1050 Bruxelles, Belgium

e-mail: thomas.wandlowski@dcb.unibe.ch; ilya.pobelov@iac.unibe.ch

Abstract. Structure transitions between copper UPD adlayers on Au(111)–(1 × 1) in sulfuric acid and chloride containing electrolyte were investigated by *in situ* scanning tunnelling microscopy. We demonstrate that co-adsorbed sulphate ions in the ($\sqrt{3} \times \sqrt{3}$)R30° UPD adlayer are replaced by chloride ions and, depending on the halide coverage, a commensurate (2 × 2) or a slightly distorted (5 × 5)-like Cu–Cl UPD adlayer are formed. The stability ranges of these phases are controlled both by the electrode potential and the Cl^- concentration. Phase transitions between the three UPD phases were monitored by time-resolved *in situ* STM. The observed structure details were attributed to mechanisms based on two-dimensional nucleation and growth processes.

Keywords. Electrochemical and time-resolved STM; Cu UPD; co-adsorption; two-dimensional phase transitions.

1. Introduction

Scanning tunnelling microscopy represents a unique tool to study steady state and dynamic processes at electrified solid/liquid interfaces with unprecedented spatial and structure resolution.[1–8] One particularly attractive class of systems represent metal adlayers prepared by underpotential deposition (UPD). This process refers to the electrodeposition of metal monolayers on a foreign metal substrate at potentials more positive than the bulk equilibrium potential on the same metal.[9] UPD is often the first step in bulk metal electrodeposition and therefore comprises a key step in electrochemical nanotechnology and many other technologically important processes.[10–12] Cu UPD on Au(hkl) and Pt(hkl) represent particularly important model systems, which are well-studied by various structure-sensitive techniques, and often served as test systems to explore new techniques in electrochemical surface science.[13–16] For example, Cu UPD on Au(111) in sulfuric acid was investigated by classical electrochemical methods[17–27] and the quartz crystal microbalance technique.[28–32] The various adlayer structures were characterized by electron diffraction,[33,34] X-ray techniques,[24,29,35–40] infrared absorption[26,40–43] and Auger electron[44] spectroscopies as well as by electrochemical STM[45–54] and atomic force microscopy (AFM).[55,56] The experimental studies are complemented by theoretical modelling employing statistical mechanics, Monte Carlo simulations, density functional and/or molecular dynamics approaches.[44,57–63]

Several groups demonstrated that anions have a strong impact on Cu UPD adlayer structures and on the phase formation kinetics (cf. reviews in refs. 15, 16). The effect of chloride on Cu UPD on Au(111), for example, was studied by voltammetry and chronocoulometry,[22,64–66] low energy electron diffraction spectroscopy,[67] X-ray absorption spectroscopy,[24,65], electrochemical STM[45,48–50,53,68–70] and AFM.[56] *In situ* STM experiments in sulfuric or perchloric acid revealed that trace amounts of chloride ions lead to the formation of an incommensurate (5 × 5)-like Cu–Cl UPD structure at high potentials.[45–47,49,50,53,68–70]. Chronocoulometric results indicated that the ratio of copper and chloride in this adlayer was equal to 1.[22,64] A bilayer structure with chloride adsorbed on top of copper is proposed.[24] The coverages of chloride and copper are approximately equal to 0·622.[2,70]

†Dedicated to the memory of the late Professor S K Rangarajan

*For correspondence

A (5 × 5)-like adlayer was also found at more negative potentials if the chloride concentration was kept above 10^{-4} M.[22,49,53,64,68–70] However, at chloride concentrations below 10^{-4} M and at low underpotentials, a (2 × 2) structure was reported, which coincides with the appearance of an additional peak in the cyclic voltammogram.[70] Based on voltammetric experiments in perchloric acid (sulphate-free electrolyte) Krznarić *et al*[66] proposed recently the existence of a third Cu–Cl UPD adlayer structure.

In the present paper, we report an *in situ* STM study on potential and time resolved structure transitions between Cu–SO_4^{2-} and Cu–Cl UPD adlayers on Au(111)-(1 × 1) electrodes. We specifically focus on the structures and stability ranges of the two (5 × 5)-like and (2 × 2) Cu–Cl UPD phases and their dependence on electrode potential and chloride concentration. We will demonstrate that the experimentally observed adlayer transitions represent mechanisms based on two-dimensional nucleation and growth processes.

2. Experimental

The Au(111) electrodes were single crystal cylinders (for cyclic voltammetry, 4 mm diameter and 4 mm height) or disks (STM studies, 10 mm diameter and 2·5 mm thickness). Before mounting the STM cell they were annealed in a hydrogen flame at red heat for 5 min, then cooled down slowly in a high purity argon stream. Subsequently, the gold electrodes were exposed for 5 min to a deoxygenated 10 mM aqueous HCl solution, which leads to the lifting of the Au(111)-($p \times \sqrt{3}$) reconstruction and to the formation of an ideally terminated Au(111)-(1 × 1) surface.

The STM measurements were carried out with a Molecular Imaging Pico-SPM employing a copper wire as reference electrode (99·999%, Aldrich). The counter electrode was a platinum wire (Goodfellow). We typically used aqueous electrolyte solutions containing 1 mM Cu^{2+} and 50 mM H_2SO_4, and added NaCl in selected experiments to reach final chloride concentrations between 10^{-4} and 10^{-6} M. The electrolyte was added into the STM cell under potential control. For further experimental details we refer to our previous paper.[53]

The electrochemical studies were conducted with an Autolab PG 300 potentiostat employing a three-compartment all-glass cell, a Pt counter and a saturated calomel reference electrode (SCE), respectively. All potentials in this paper are quoted with respect to the SCE.

All solutions were prepared with Milli-Q water (18·2 MΩ·cm, 2–3 ppb TOC), and with suprapure Merck reagents, except for CuO, which was purchased from Sigma-Aldrich (99·9999%). The glassware and the STM cell (Kel-F) were cleaned by soaking in caroic acid, followed by multiple rinsing cycles with Milli-Q water.

Throughout the paper, the absolute coverage values θ are given with respect to the density of atoms on the Au(111)–(1 × 1) surface. A relative coverage θ_r is taken as a ratio of the area occupied by the corresponding phase either to the total area or to the maximum area occupied by the given phase.

3. Results and discussion

3.1 *Electrochemical properties*

Cyclic voltammetry was applied first to explore the concentration effect of Cl^- ions on the UPD of copper on Au(111)–(1 × 1) in 0·05 M H_2SO_4 (figure 1). The cyclic voltammogramm (CV) of the chloride-free electrolyte (trace 1) shows two characteristic pairs of peaks P_1/P_1' and P_2/P_2' separating a region I of disordered sulphate and copper ion adsorption positive of P_1/P_1', which is followed by the stability range of the well-known Cu UPD ($\sqrt{3} \times \sqrt{3}$)R30° phase (between P_1/P_1' and P_2/P_2'). A SXS study of Toney *et al* revealed that copper ions form a commensurate honeycomb lattice (occupation of three-

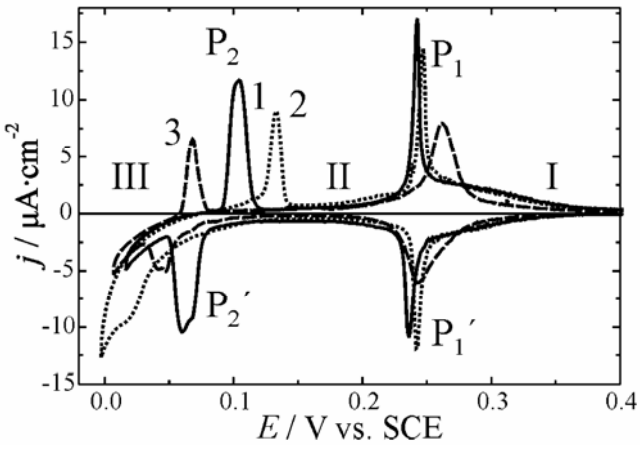

Figure 1. Cyclic voltammogram of a Au(111)–(1 × 1) electrode in 0·05 M H_2SO_4 + 1 mM Cu^{2+} + x M Cl^-, scan rate 1 mV s^{-1}, x: (1, solid) 0, (2, dotted) 5×10^{-6} (3, dashed) 5×10^{-5}.

fold hollow sites, 2/3 coverage) with sulphate species coadsorbed in the centers (1/3 coverage) above the plane of the copper species.[38] At E negative of P_2/P_2' the Cu UPD (1×1) phase is formed onto which bulk copper deposition proceeds at even more negative potentials.[14,16,17] Addition of a small amount of Cl^- ions such as 5×10^{-6} M (curve 2 in figure 1), leads to a slight positive shift of the positions of P_1/P_1' and P_2/P_2'. This trend continues with increasing Cl^- concentration for P_1/P_1', while P_2/P_2' shifts towards more negative potentials. Simultaneously, the hysteresis between P_2 and P_2' decreases. At low chloride concentrations, this hysteresis depends on the stirring of the solution, therefore reflecting diffusion-controlled mass transport.[66] However, at $c(Cl^-) > 10^{-5}$ M this effect is less pronounced clearly reflecting intrinsic kinetic limitation of a surface-confined phase formation process.

This qualitative description of the CV's plotted in figure 1 illustrates the pronounced influence of Cl^- ions on the Cu UPD on Au(111)–(1×1) in 0·05 M H_2SO_4, even at Cl^- concentrations 4 orders of magnitude lower than sulphate. The complex potential dependence of the positions of P_1/P_1' and P_2/P_2' reveals the existence of various chloride and sulphate ion containing Cu UPD adlayers.[15,66,70] For didactic reasons and as a guidance for the subsequent discussion, we introduce three characteristic potential regions, I to III, which are separated by the characteristic pairs of peaks P_1/P_1' and P_2/P_2'.

3.2 *Steady STM results*

No ordered adlayers were found in region I at potentials more positive than P_1/P_1'. Chronocoulometric measurements revealed the potential-dependent co-adsorption of Cu^{2+}, SO_4^{2-} and Cl^- ions. In the following sections we will describe structure details of three Cu UPD phases resolved in potential regions II and III, and comment on the existence of an additional adlayer in region III.

3.2a *Phase 1:* Figure 2a shows a high-resolution image of the commensurate Cu UPD ($\sqrt{3} \times \sqrt{3}$)R30° adlayer in chloride-free electrolyte. The nearest-neighbour spacing of the hexagonally arranged bright features, the latter represent the co-adsorbed sulphate species,[19,20,38] is estimated as 0·49 × 0·03 nm with a characteristic angle $\alpha = 60 \pm 4°$. The apparent corrugation height varies between 0·05 and 0·07 nm. Figure 2b illustrates rotation domain boundaries with typical rotation angles of 120° and a spacing of ≈1 nm between adjacent domains. Both features indicate the mismatch of the occupied sublattices in different growth domains and the commensurability with the hexagonal substrate lattice. The incomplete rows predict a linear line-by-line growth process at step edges.

3.2b *Phase 2:* Figure 3a and b illustrate an intermediate and a high resolution image of the Cu

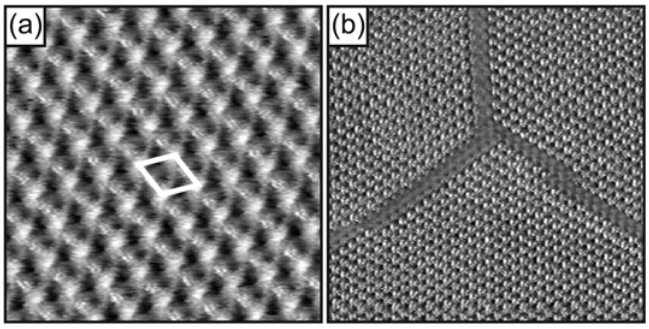

Figure 2. ($\sqrt{3} \times \sqrt{3}$)R30° Cu–SO_4^{2-} UPD adlayer 1 in 0·05 M H_2SO_4 + 1 mM Cu^{2+}: (**a**) 4 × 4 nm, E_s = 0·17 V, E_t = 0·01 V, I_T = 0·4 nA. The unit cell is shown. (**b**) 15 × 15 nm, E_s = 0·16 V, E_t = 0·03 V, I_T = 0·3 nA. Rotation domain boundaries are seen.

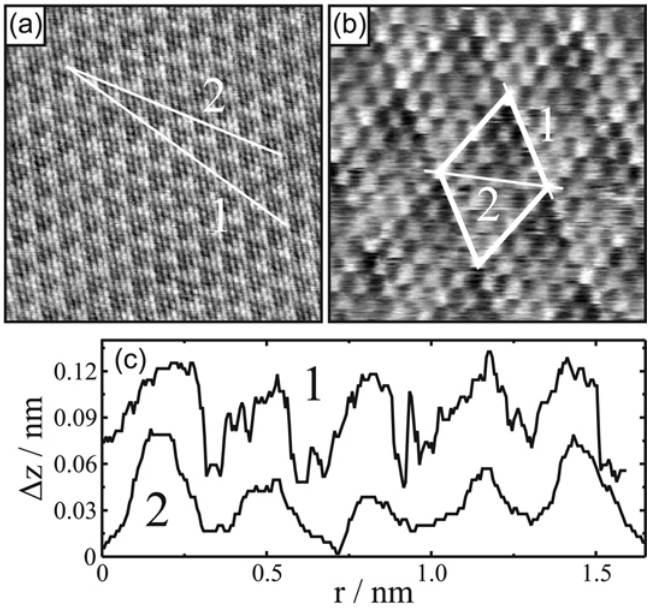

Figure 3. (5 × 5) Cu–Cl UPD adlayer 2 in 0·05 M H_2SO_4 + 1 mM Cu^{2+} + 5×10^{-5} M Cl^-: (**a**) 15 × 15 nm, E_s = 0·11 V, E_t = 0·01 V, I_T = 2·5 nA. The lines show the characteristic directions of the Moiré pattern (1) and of the atomic features (2). (**b**) 4 × 4 nm, E_s = 0·11 V, E_t = 0·01 V, I_T = 2 nA. The unit cell is indicated. (**c**) two cross-sections of line profiles indicated in (**b**), vertically shifted for clarity.

UPD adlayer recorded in region II for Au(111)–(1 × 1) and 1 mM Cu^{2+} + 0·05 M H_2SO_4 in the presence of 5×10^{-5} M chloride. This contrast pattern, which is typical for chloride concentrations higher than 10^{-5} M, could only be resolved at rather high tunnelling currents ranging between 1 to 3 nA. We did not observe any domain boundaries. However, figure 3a shows a distinct hexagonal Moiré motive, which reflects a slight rotation between the adlayer and the substrate. The periodicity and the characteristic angle of the Moiré pattern are estimated to $d_M = 1{\cdot}5 \pm 0{\cdot}05$ nm and $\gamma = 60 \pm 3°$ at $E = 0{\cdot}11$ V. The corrugation difference between bright and dark spots amounts to 0·05 nm. We notice that the main lattice directions of the Moiré pattern (cf line 1 in figure 3a) are rotated by $13 \pm 2°$ as referred to the direction of the atomically resolved features of the Cu UPD adlayer (line 2 in figure 3a).

High-resolution images (figure 3b) revealed a close-packed adlayer with an apparent rhombohedral unit cell. The characteristic angle is $\alpha = 60 \pm 5°$ and the unit cell vectors are $a = b = 1{\cdot}44 \pm 0{\cdot}04$ nm at $E = 0{\cdot}11$ V and $1{\cdot}56 \pm 0{\cdot}04$ nm at $E = 0{\cdot}21$ V. The corresponding distances d between atomic features, which represent the positions of the chloride ions,[15] were estimated to $0{\cdot}36 \pm 0{\cdot}01$ nm and to $0{\cdot}39 \pm 0{\cdot}01$ nm, respectively. The contrast modulation within the atomic rows is not uniform. Figure 3b shows cross-sections of the adlayer in two characteristic hexagonal directions. The atomic features along trace 1 reveal a nearly constant apparent corrugation height. Trace 2 shows a distinct modulation of peak heights by 0·04 nm with a minimum approximately in the 'center' of the rhombohedral unit cell.

Our experimental observations are in agreement with basic properties of the (5 × 5)-like Cu UPD in chloride containing electrolyte as reported in refs. 45, 48, 56, 68, 69. The structure is assumed to be represented by a 1 : 1 bilayer with chloride placed on top of the copper ions. However, there are also several distinct differences. The interatomic distances were reported in ref. 56 and ref. 70 to be potential independent in the entire range of region II. On the other hand, Batina *et al*[49], Ikemiya *et al*[56] and we observed a significant potential dependence ranging from $0{\cdot}39 \pm 0{\cdot}01$ nm near P_1/P_1' to $0{\cdot}36 \pm 0{\cdot}01$ nm at potentials close to P_2/P_2'. This potential dependence is also reflected in different characteristic distances of the reported Moiré structure. While in this study and in ref. 49 a value $d_M = 1{\cdot}5 \pm 0{\cdot}05$ nm was found, a value of 1·2 nm was determined in other works.[53,70] We propose that the Cu–Cl UPD phase II represents either an incommensurate adlayer or can be represented by slightly different coexisting local lattices with a potential dependent distribution. The discussion of chronocoulometric and EXAFS data as communicated by Wu *et al* (ref 65) supports this interpretation. The distribution of coexisting structures can be affected by the preparation conditions such as the nature and concentration of reactants, electrode potential, and generally by the 'history' of the particular adlayer.

3.2c *Phase 3:* At low Cl^- concentrations ($<10^{-5}$ M) and at potentials more negative than 0·11 V (e.g. at $E < P_2$ for the dotted curve plotted in figure 1), a new adlayer labelled phase 3 was discovered (figure 4). We observed frequently translation (figure 4a) and rotation domain boundaries with characteristic angles of multiples of 60°. A Moiré pattern was not found. High resolution images such as shown in figure 4b revealed a hexagonal symmetry pattern with a characteristic lattice constant $a = 0{\cdot}59 \pm 0{\cdot}02$ nm and an angle $\alpha = 60 \pm 5°$. Referring to an *in situ* STM study of Cu UPD in perchloric acid[70] and to chronocoulometric data[64] we attribute the observed structure to a (2 × 2) adlayer (figure 4c). The unit

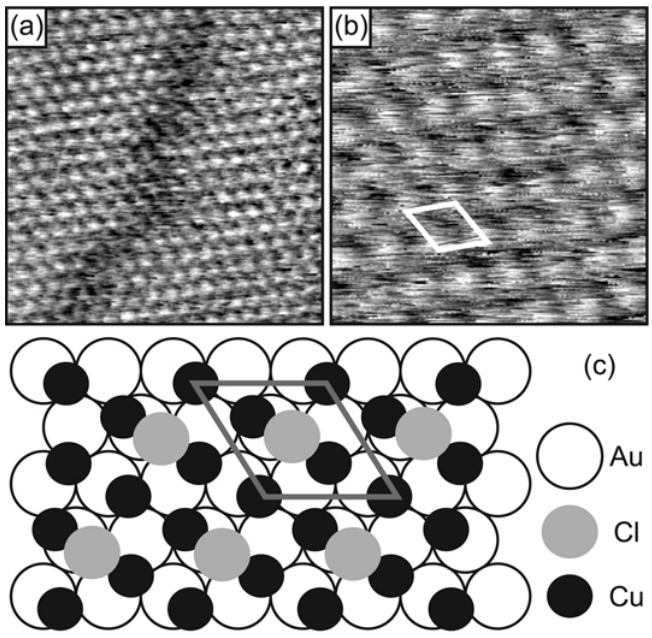

Figure 4. (2 × 2) Cu–Cl UPD adlayer 3 in 0·05 M H_2SO_4 + 1 mM Cu^{2+} + 10^{-5} M Cl^-: (**a**) 10 × 10 nm, $E_s = 0{\cdot}08$ V, $E_t = 0$ V, $I_T = 0{\cdot}26$ nA. A 'frizzy' domain boundary is also seen. (**b**) 4 × 4 nm, $E_s = 0{\cdot}08$ V, $E_t = 0$ V, $I_T = 0{\cdot}26$ nA. The unit cell is shown (**c**) model of the (2 × 2) phase.[70]

cell consists of a layer of copper ions residing on the Au(111) substrate and Cl^- anions coadsorbed on top. The Cu ions are slightly displaced from the three-fold hollow site positions of the underlying Au(111) substrate. One unit cell is represented by three copper and one chloride ion resulting in a coverage $\theta_{Cu} = 0{\cdot}75$. The structure is stabilized by one Cl^- anion co-adsorbed in the center of the unit cell. The latter appears to be observed as protrusion in the STM contrast pattern. The corresponding coverage of the chloride in phase 3 is giving to $\theta_{Cl} = 0{\cdot}25$.

3.2d *Other interfacial phases:* At high chloride concentrations ($>10^{-5}$ M) and at potentials more negative than P_2/P_2' we[53] and others[49] found a second (5 × 5)-like STM contrast pattern with a well-resolved Moiré pattern (characteristic distance $d_M = 1{\cdot}2$[53] respective 1·5 nm[49]) rotated 14° with respect to the atomic lattice directions. However, we did not succeed in this work to obtain a high resolution contrast pattern of individual chloride (respective copper) ions, and are therefore not able to report further structure details of the high coverage chloride adlayer at $E < P_2/P_2'$.

3.3 *Phase transitions*

We have applied time-resolved *in situ* STM to study two-dimensional phase transitions between Cu UPD adlayers in 0·05 M H_2SO_4 + 1 mM Cu^{2+} + 10^{-5} M NaCl. This approach provides direct access to potential-induced structure changes of the respective adlayer phases 1, 2 and 3. We also notice that the experimentally accessible STM contrast pattern represents the positions of the anions, and does not provide direct access (at least under electrochemically accessible tunnelling conditions) to the positions of individual copper species.

The results reported in section 3·2 also demonstrate that the structure transitions between the various Cu UPD adlayers involve changes of the coverages of the adsorbed copper ions as well as of the two anions. The bulk concentration of Cu^{2+} and SO_4^{2-} ions are kept sufficiently high, which allows neglecting kinetic limitations due to bulk diffusion of the respective species to the surface.

3.3a *Transitions between the (2 × 2) and the (5 × 5)-like adlayers of phases 3 and 2:* A steady state (2 × 2) Cu UPD adlayer (phase 3) was formed at $E = 0{\cdot}03$ V on an unreconstructed Au(111)–(1 × 1) electrode (potential region III in figure 1). The STM contrast of this phase appears bright and rather uniform. The transition to the (5 × 5)-like adlayer (phase 2) was initialized upon stepping the substrate potential to 0·16 V (potential region II in figure 1). The line in figure 5a indicates the position at which the potential step was applied. Patches of the new phase 2, characterized by a slightly darker contrast as compared to phase 3 and a characteristic Moiré pattern, appear immediately after the potential step. Initial patches of phase 2 are separated by 'channels' and 'holes' of darker contrast. The holes

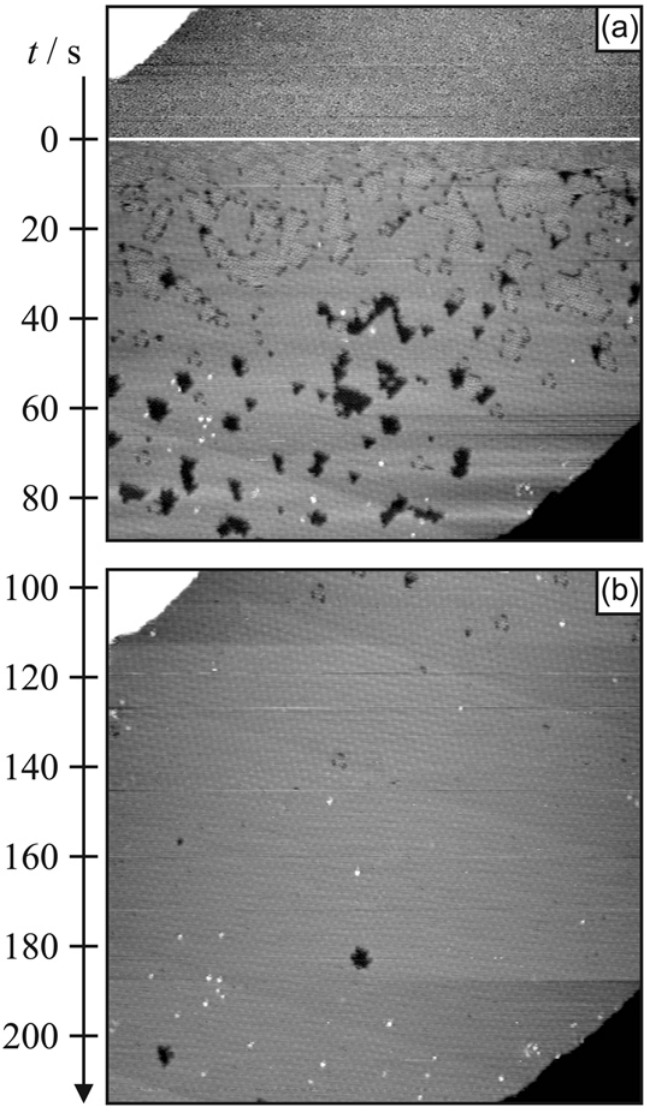

Figure 5. (**a**) Transitions of the Cu–Cl (2 × 2) phase into the (5 × 5) phase as triggered by a single potential step from $E_i = 0{\cdot}03$ V to $E_f = 0{\cdot}16$ V. The position at which the potential step was applied is indicated by the line. (**b**) Same area scanned after 100 s. Imaging conditions: size 80 × 80 nm, $E_t = 0{\cdot}02$ V, $I_T = 0{\cdot}33$ nA.

are 0·10 to 0·12 nm deep and reveal inside the characteristic ($\sqrt{3} \times \sqrt{3}$)R30° pattern of the chloride-free UPD phase 1. With time the patches of phase 2 increase in size until they cover the entire electrode surface. Simultaneously, we observed an initial expansion of the 'dark holes'. However, upon the complete disappearance of patches of the initial (2 × 2) Cu UPD phase these holes shrink and transform completely into the (5 × 5)-like UPD adlayer 2 (figure 5b). We notice that the boundaries between the growing islands of phase 2 and the holes (phase 1) exhibit characteristic hexagonal symmetry elements of the underlying substrate throughout the entire transformation.

Our experimental observations could be rationalized as follows: islands of the 1 : 1 bilayer with chloride being on top of copper ions (phase 2) form immediately after the potential step to 0·16 V according to a nucleation process. The growth of this phase proceeds by rearrangement of the Cu–Cl UPD layer 3, specifically by the partial desorption of Cu^{2+} and the incorporation of additional Cl^- ions. However, the surface concentration of Cl^- ions is initially too low to cover the entire surface. In consequence, excess Cu^{2+} ions form temporarily 'dark' patches of the ($\sqrt{3} \times \sqrt{3}$)R30° Cu–SO_4^{2-} UPD phase 1. This process is triggered by the higher solution concentration of SO_4^{2-} as compared to Cl^-. Upon increasing the surface concentration of Cl^-, as a result of a bulk-diffusion limited process, the sulphate ions of the ($\sqrt{3} \times \sqrt{3}$)R30° Cu UPD phase 1 will be replaced by newly adsorbed Cl^- ions, which leads to the healing out of the 'dark holes' and to the formation of a long range ordered phase 2 without any detectable domain boundaries. This exchange proceeds at the periphery of the growing islands. The growths directions follow the symmetry of the substrate surface.

A structure transition between a (2 × 2) and a (5 × 5)-like Cu UPD adlayer as governed by the diffusion limited transport of Cl^- ions was also reported in perchlorate solutions in the presence of trace amounts of Cl^-.[70]

Figure 6 illustrates the reverse transition from the (5 × 5)-like (phase 2) to the (2 × 2) (phase 3) Cu UPD adlayer upon application of a potential step from 0·25 V to 0·08 V. The nucleation of the new phase starts after an induction period at defects such as step edges (upper right in figure 6). If choosing slightly higher final potentials, one also observes occasionally growing islands of the (2 × 2) phase 3 on terrace sites. However, the growth rate is rather high, which prevented us from resolving additional structure details. The 'smooth' phase 2 with its characteristic Moiré pattern quickly transforms into the somewhat 'rougher' phase 3. Simultaneously, domain boundaries such as shown in figure 6 appear.

In reference to the structure models described in section 3.2, the transition of phase 2 into phase 3 involves the desorption of Cl^- ions accompanied by an increase of the Cu^{2+} adlayer concentration. Both processes are not limited by bulk diffusion. The overall kinetics is controlled by nucleation and growth of the new (2 × 2) Cu UPD adlayer.

At this stage, we would like to discuss the possibility of tip effects on the kinetics of the experimentally observed phase transitions. The electrostatic field as induced by the tip may affect the local potential at the interface. However, the bias voltage of 0·1 V applied to the interface over a tip-substrate distance of a few nanometers results in an electric field strength of $\approx 10^{-10}$ V m^{-1}, which is one order of magnitude lower than typical electric fields existing in the electrochemical double layer. A negligible electrostatic field effect was also concluded in,[70] where the same transition potentials between the phases 2 and 3 were derived from both CV measurements and STM observations. We also reject the possibility of a mechanical interaction between the tip and the adlayer. By studying the set-point dependence of the

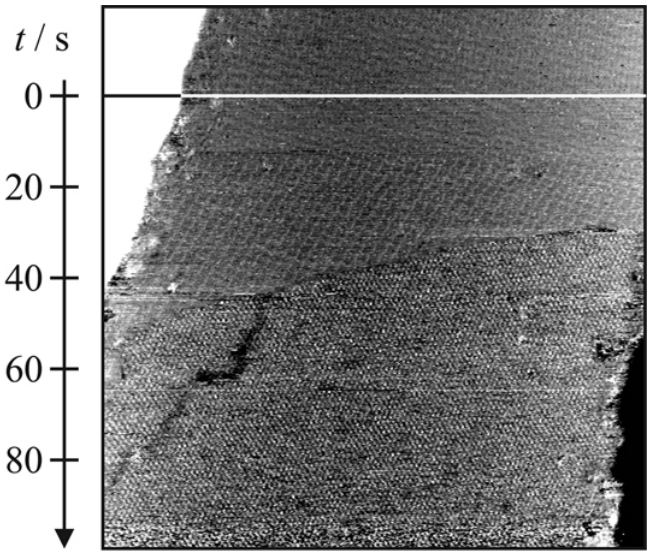

Figure 6. Transition of the (5 × 5) into the (2 × 2) Cu–Cl UPD phase triggered by a single potential step from $E_i = 0.25$ to $E_f = 0{\cdot}08$ V. Size 60 × 60 nm, $E_t = 0{\cdot}01$ V, $I_T = 0{\cdot}27$ nA. The position at which the potential step was applied is indicated by the horizontal line.

STM images, it was shown that an increase of the tunnelling current to $I_T > 10$ nA (i.e. a decrease of tip-substrate separation) causes a distortion of the adlayer phase 1.[52,53] Typical values of I_T used in this study are much smaller, and no indications of perturbed images were found.

Another effect is the geometric shielding of the surface underneath the STM tip, which could hinder the diffusion of Cl^- ions. One may expect that the shielding may modify the diffusion rate and not affect the mechanism of the process. Krznarić *et al*[66] carried out CV measurements for the transition from phase 3 to phase 2 in perchlorate electrolyte under conditions of an enhanced mass transport (by stirring the electrolyte), and concluded that mass transport has no effect. This result differs from observations based on *in situ* STM measurements (this work and ref. 70) and may indicate a hindering of the diffusion of a minority species due to shielding by the tip in the STM configuration.

3.3b *Structure transition between the SO_4^{2-} and Cl^- containing UPD adlayers:* Based on surface excess data as derived from chronocoulometric experiments[64] and in agreement with observations from cyclic voltammetry one observes that the onset of formation of both the sulphate and the chloride containing Cu UPD phases 1 and 2 takes place at ca. 0·26 V. The maximum surface excess of the two anions was obtained at $E \approx 0{\cdot}1$ and $E \approx 0{\cdot}15$ V, respectively. The replacement of the $(\sqrt{3} \times \sqrt{3})R30°$ Cu UPD sulphate phase 1 by the (5×5)-like chloride phase 2 was mentioned in[45,46,48,56] but not studied in detail. These authors suggested that the replacement of SO_4^{2-} by Cl^- is rather slow at the onset of copper deposition, but accelerates significantly at lower potentials.

We studied the replacement of SO_4^{2-} on top of the Cu UPD layer by Cl^- employing *in situ* STM in 0·05 M H_2SO_4 + 1 mM Cu^{2+} and 10^{-5} M Cl^- (figure 7). A long range ordered $(\sqrt{3} \times \sqrt{3})R30°$ Cu-SO_4^{2-} UPD adlayer phase 1 was created immediately after stepping the potential from 0·35 V to 0·23 V. The transition into the Cl^- containing UPD adlayers was triggered by a second step to a more negative potential such as $E_f = 0{\cdot}11$ V. The new phase was recognized by a brighter contrast of characteristic apparent height. The Cl^- containing phase is formed preferentially at substrate and adlayer defects such as steps and domain boundaries (figure 7a) at potentials rather close to the positions of P_1/P_1' (figure 1). At more negative final potentials we also observed the nucleation of islands of the new Cu–Cl UPD phase on terrace sites. The growth follows the characteristic symmetry directions of the hexagonal substrate. We frequently observed triangular islands which subsequently merge to form large patches of the Cl^- containing UPD phase. Growth proceeds by anion exchange at step edges.

A detailed inspection of the freshly formed Cu–Cl UPD patches, which appear bright in the STM contrast, reveal a certain roughness and many translation domain boundaries (figure 7b and c). Clearly, this adlayer corresponds to the (2×2) Cu–Cl UPD phase 3. Subsequently, this structure transforms into the chloride-rich (5×5)-like UPD phase 2 (figure 7d and e) as demonstrated by the appearance of the characteristic Moiré pattern (cf figure 3) and a smoother texture accompanied with the disappearance of domain boundaries of the intermediate (2×2) adlayer. The patches of three different adlayers involved in this transition are labelled in figure 7.

In an attempt to quantify the overall kinetics of the structure transition between the SO_4^{2-} containing $(\sqrt{3} \times \sqrt{3})R30°$ phase 1 into the two Cu UPD chloride phases 3 respective 2, we introduce θ_r as the relative coverage. θ_r was estimated from each image as a ratio of the area occupied by the Cu–Cl UPD phases and the total area of the entire terrace. The time corresponding to the tip positioned in the middle of the imaged area was used as a temporal coordinate. Figure 7g illustrates the evolution of the relative coverages θ_r (2×2) (curve 1) and θ_r (5×5) (curve 2) for a potential step from $E_i = 0{\cdot}23$ V to $E_f = 0{\cdot}11$ V. Initially the intermediate phase 3 grows, then its coverage passes a maximum and it subsequently decreases to zero upon the transformation of the (2×2) into the (5×5) Cu–Cl UPD adlayer. Qualitatively, the shapes of these two curves resemble the kinetic curves of two subsequent irreversible reactions. The latter is formed after an induction period. Figure 7b and c suggest that sufficiently large patches of phase 3 are required for the nucleation of phase 2. Once formed, the patches of phase 2 are quickly expanding over the areas occupied by phase 3 as well as by the chloride-free phase 1. The time dependence of formation of the (5×5) Cu–Cl UPD layer can be represented by the Avrami-type equation 1:[16]

$$\theta_r = 1 - \exp(-b_f t^m), \quad (1)$$

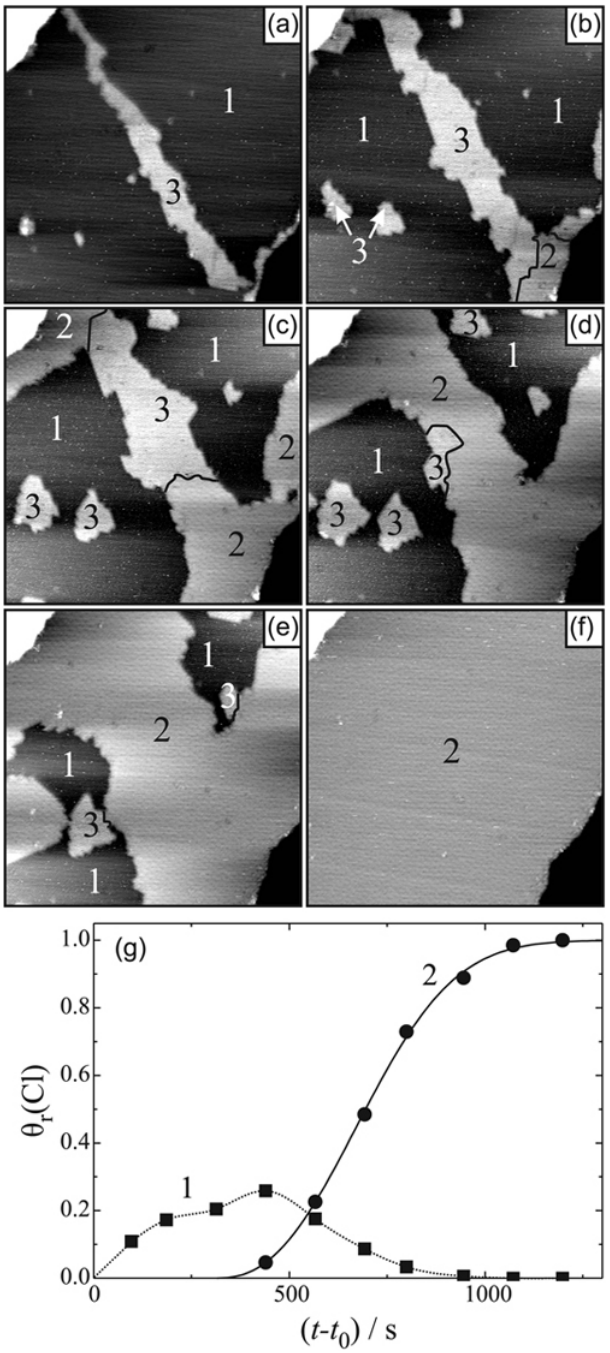

Figure 7. Sequence of STM images recorded after a single potential step from $E_i = 0{\cdot}23$ V ($(\sqrt{3} \times \sqrt{3})$R30° Cu–$SO_4^{2-}$ UPD phase) into the stability range of the Cu–Cl UPD phases ($E_f = 0{\cdot}11$ V). Image size 65 × 65 nm, $E_t = 0{\cdot}025$ V, $I_T = 0{\cdot}2$ nA, (**a**) $t = 0$ min; (**b**) $t = 4$ min; (**c**) $t = 8$ min; (**d**) $t = 10$ min; (**e**) $t = 12$ min; (**f**) $t = 20$ min. The three adlayer phases involved are labeled by the corresponding numbers. The borders between phases 2 and 3 are marked by additional lines. (**g**) Time-dependent evolution of the relative coverages of the (2 × 2) (■) and of the (5 × 5)-like (●) Cu UPD phases. The dotted line is a guide to the eyes. The solid line represents the fit of (2) to the experimental θ_r (5 × 5) – t dependence. The corresponding parameters are $J = 1{\cdot}2$ s^{-1} and $A = 6{\cdot}9 \times 10^{-6}$ s^{-2}.

b_f is a constant incorporating both rates of nucleation and growth, and m representing the sum of dimension and the time exponent in the nucleation law. A nonlinear regression fit of (1) to the experimental θ_r (5 × 5) – t dependence results in $m \approx 2{\cdot}5$. Non-integer values of the Avrami-exponent m ranging between 2 and 3 point to a mechanism based on an exponential law of nucleation in combination with a linear growth process.[16] This regime is represented by (2):

$$\theta_r = 1 - \exp(-A\{t^2 - 2t/J + 2/J^2[1 - \exp(-Jt)]\}), \quad (2)$$

where J is the rate constant of nucleation and A is a constant incorporating the maximum number of nucleation sites and a rate constant of growth. The fit of (2) to the experimental θ_r (5 × 5) – t dependence is shown by the solid line in figure 7g.

The transformation of the SO_4^{2-} containing $(\sqrt{3} \times \sqrt{3})$R30° phase 1 into the two Cu–Cl UPD adlayers was studied at different final potentials. For an electrolyte solution containing 0·05 M H_2SO_4 + 1 mM Cu^{2+} + 10^{-5} M Cl^- the three UPD phases coexist temporarily only around $E \approx 0{\cdot}11$ V. This potential coincides approximately with the position of the pair of peaks labelled P_2/P_2' in figure 1, which separates the previously introduced potential regions II and III. At potentials more positive of P_2/P_2', the rate of formation of the (5 × 5) Cu–Cl UPD phase initially increases, but subsequently decreases due to the competition with the Cu–SO_4^{2-} UPD adlayer 1. At potentials close to P_1/P_1', a long-time coexistence of both phases 1 and 2 could be observed. On the other hand, at lower final potentials ($E_f < P_2/P_2'$), such as $E_f = 0{\cdot}08$ V, we only observed the formation of phase 3 and no subsequent transformation into the (5 × 5) Cu–Cl phase 2 took place.

Figure 8 shows a plot of θ_r vs $(t - t_0)$ for experimental transients with $E_i = 0{\cdot}24$ V to two final potentials into the stability range of the Cu–Cl UPD adlayers 2 or 3. The time required to reach quasi-stationary conditions varies up to an order of magnitude. Transient 1 ($E_f = 0{\cdot}08$ V) is formally represented well by equation (3):

$$\theta_r = 1 - \exp[-k(t - t_0)]. \quad (3)$$

Deviations exist for transient 2. Choosing $E_f = 0{\cdot}16$ V leads for $t > 2000$ s to a quasi-stationary coexistence of the SO_4^{2-} containing $(\sqrt{3} \times \sqrt{3})$R30° phase 1 and of the Cl-rich (5 × 5) Cu–Cl UPD phase. However, the rate (3) is still applicable if one

considers the steady state area occupied by the Cu–SO_4^{2-} UPD phase 1 as a reduction of the effective electrode area.

An exponential-type $\theta_r - t$ dependence may represent two different mechanisms:[16] (i) a slow adsorption process or (ii) instantaneous nucleation in combination with surface diffusion-controlled growth. The adsorption process, which, for the present system, corresponds to the slow anion replacement, is a homogeneous process. In other words, one should expect an equal distribution of the new phase over the entire surface. Instead, we observed the formation, growth and merging of trigonal islands of the Cu–Cl UPD phases on defects of the substrate surface and in the seed adlayer, and occasionally few (in the sequence shown in figure 7 just two) additional islands form on terrace sites. We conclude that the potential-induced two-dimensional phase transition of the Cu–SO_4^{2-} UPD adlayer into one of the Cu–Cl UPD phases proceeds according to a nucleation-and-growth controlled mechanism.

3.3c *Replacement of the (5 × 5)-like Cu–Cl UPD layer 2 by the (√3 × √3)R30° Cu–SO_4^{2-} UPD phase 1:* The transition of the (5 × 5)-like Cu–Cl adlayer into the (√3 × √3)R30° Cu–SO_4^{2-} UPD phase 1 could only be observed when starting the experiment with a freshly formed (5 × 5)-like phase 2. The following protocol was applied: the substrate potential was first set to 0·03 V to form the (2 × 2) Cu–Cl UPD phase 3. Subsequently, the potential was stepped to 0·16 V and kept there for several minutes until a long range ordered (5 × 5) Cu–Cl UPD phase 2 is established (bright contrast in figure 9a). Finally, the potential was advanced to E_f = 0·24 V (e.g. close to P_1/P_1'), which is close to the positive stability edge of formation of an ordered Cu UPD adlayer under the present experimental conditions. Figure 9 illustrates the time-dependent evolution of the adlayer structure following this last potential step. The structure transition at E_f = 0·24 V starts with the formation of 'holes' at steps and adlayer defects.

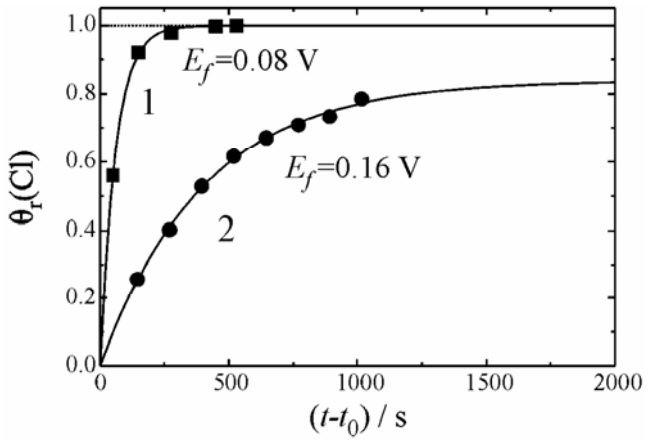

Figure 8. θ_r vs t traces after a potential step from E_i = 0·24 V (Cu–SO_4^{2-} UPD phase) to two final values E_f. The points show the experimental coverage data, and the solid lines are the fits according to (3) (1) 1 to 3; E_f = 0·08 V, k = 0·0164 s^{-1}; (2) 1 to 2; E_f = 0·16 V, k = 0·0025 s^{-1}.

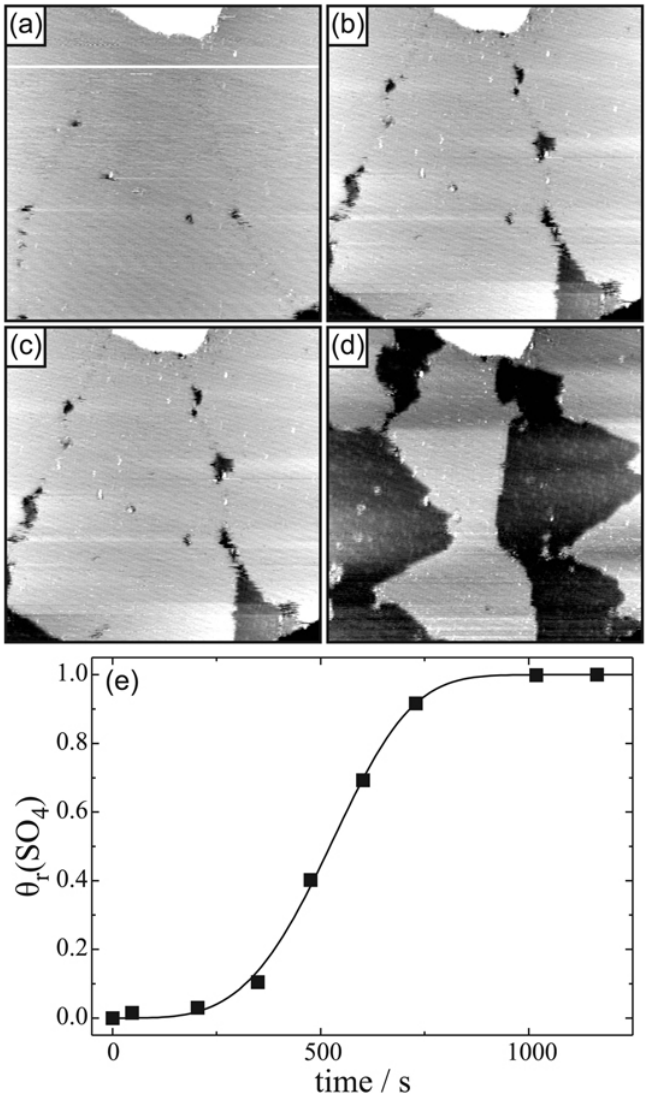

Figure 9. Time dependent STM images after a potential step from E_i = 0·16 V ((5 × 5)-like Cu–Cl UPD phase 2) towards E_f = 0·24. Size 100 × 100 nm, E_t = 0·01 V, I_T = 0·2 nA. (**a**) t = 0 min, (**b**) t = 4 min, (**c**) t = 6 min, (**d**) t = 8 min. (**e**) Time dependent evolution of the relative surface coverage of the Cu-SO_4^{2-} UPD phase (■). The solid line represents the fit of (1).

The latter are seen in figure 9a to c as two lines of small growing patches of the $(\sqrt{3} \times \sqrt{3})$R30° Cu–$SO_4^{2-}$ UPD phase 1 within the adlayer 2. Their growth leads to a triangular shape, and growing patches start to merge (figure 9d). After approximately 15 min, no further changes of the interfacial structure could be observed. A steady state of coexisting areas of the two Cu UPD phases 1 and 2 is established. We notice that no complete substitution of chloride by sulphate was observed at chloride concentrations $\geq 10^{-5}$ M. However, there is clear evidence that the equilibrium is completely shifted towards the Cu–SO_4^{2-} UPD phase for Cl^- concentrations less than 10^{-6} M.

Figure 9e illustrates the time-dependent evolution of the relative coverage of the Cu–SO_4^{2-} UPD phase, θ_r (with reference to the maximum equilibrium coverage at $E_f = 0{\cdot}24$ V, cf. figure 9d). This plot could be represented formally by an Avrami-type (1). A nonlinear regression fit of (1) to the experimental data plotted in figure 9e leads to $b_f = 2{\cdot}66 \times 10^{-11}$ s^{-m} and $m = 3{\cdot}8 \pm 0{\cdot}2$. The latter suggests a 'hole' nucleation process according to a power law[71]. An Avrami exponent $m = 4$ could represent a 2-step nucleation process (to form a stable 'hole' of the Cu–SO_4^{2-} UPD phase 1) in combination with a 2D linear growth law or 3-step nucleation coupled with surface-diffusion controlled growth.[16] The regular shape of the growing patches of the SO_4^{2-} containing Cu UPD adlayer 1 suggests that the data plotted in figure 9 could be represented best by the first mechanism, which assumes a linear law of growth.

4. Conclusions

The interfacial structures of potential-induced Cu UPD adlayers on Au(111)–(1×1) were studied in 0·05 M H_2SO_4 in the presence of co-adsorbed Cl^- ions by cyclic voltammetry, steady-state and time-resolved *in situ* STM.

The cyclic voltammograms of the studied systems showed two pairs of peaks P_1/P_1' and P_2/P_2', which separate, depending on the Cl^- concentration, three interfacial regions of Cl^- ((2×2) adlayer at E negative of P_2/P_2' and (5×5)-like adlayer at E between P_2/P_2' and P_1/P_1') and SO_4^{2-} (at E between P_2/P_2' and P_1/P_1' in the absence of Cl^-) containing Cu UPD phases on Au(111)–(1×1). The structures of the three Cu UPD adlayers were obtained with atomic resolution. The distinct differences in the STM contrast patterns of the three Cu UPD phases allowed to monitor *in situ* the time-dependent evolution of potential-induced structure changes within these adlayers.

The transformation of the (2×2) Cu–Cl UPD phase 3 into chloride-rich (5×5)-like phase 2 proceeds in the presence of an excess of SO_4^{2-} ions via intermediate $(\sqrt{3} \times \sqrt{3})$R30° Cu–$SO_4^{2-}$ UPD 'hole patches', which finally transform into the (5×5)-like phase 2 controlled by the slow surface diffusion of Cl^- ions. The reversed process ((5×5)-like to (2×2) Cu–Cl UPD phase 3) is controlled by a preferential nucleation of the new phase at substrate surface and adlayer defect sites. Rarely we observed growing islands on terraces.

The potential-induced replacement of the Cu–SO_4^{2-} UPD phase 1 by the Cl^- containing Cu UPD adlayers was studied in detail in the presence of low Cl^- concentrations ($\leq 10^{-5}$ M). The STM experiments reveal that nuclei of the new phase form at defect sites of the substrate surface (steps, kinks) or within the initial adlayer (domain boundaries). Occasionally, we also observed nuclei on smooth terrace sites. The nuclei formed are growing until they coalesce. The growing patches exhibit a characteristic triangular shape reflecting the main symmetry directions of the underlying substrate surface. These observations correspond to a heterogeneous nucleation and a directional lateral propagation of the new phase. Depending on the final potential, we either observed the exclusive formation of the (2×2) Cu–Cl phase 3, the transient formation of the (2×2) phase and its subsequent transformation into a (5×5) Cu–Cl adlayer 2, or (at more positive potentials in region II) the establishment of a steady-state coexistence between the (5×5) Cu–Cl and the $(\sqrt{3} \times \sqrt{3})$R30° Cu-$SO_4^{2-}$ phases.

By choosing a low Cl^- concentration and a proper potential program with final potentials around P_1/P_1', we also explored the time-dependent evolution of the replacement of a (5×5)-like Cu–Cl UPD phase 2 by the sulphate-containing $(\sqrt{3} \times \sqrt{3})$R30° Cu UPD phase 1. The underlying kinetic law seems to follow a multi-step hole nucleation in combination with a linear growth regime.

Our results illustrate the complex interplay of sulphate and chloride containing Cu UPD adlayers, and confirm a much stronger co-adsorption of chloride with copper as compared to sulphate, even at concentrations 4 orders of magnitude lower. The steady state UPD structures as well as the observed nucleation and growth pattern show characteristic symmetry elements of the underlying hexagonal Au(111)-(1×1) substrate surface.

Acknowledgements

This work was supported by Research Center Jülich and the University of Bern. I V P also acknowledges support of Deutscher Akademischer Austausch Dienst (DAAD) for a Ph D Fellowship.

References

1. Liu H Y, Fan F R F, Lin C W and Bard A J 1986 *J. Am. Chem. Soc.* **108** 3838
2. Lustenberger P, Rohrer H, Christoph R and Siegenthaler H 1988 *J. Electroanal. Chem.* **243** 225
3. Wiechers J, Twomey T, Kolb D M and Behm R J 1988 *J. Electroanal. Chem.* **248** 451
4. Gewirth A A and Niece B K 1997 *Chem. Rev.* **97** 1129
5. Itaya K 1998 *Prog. Surf. Sci.* **58** 121
6. Kolb D M 2001 *Angew. Chem. Int. Ed.* **40** 1162
7. Kolb D M 2002 *Surf. Sci.* **500** 722
8. Wang D and Wan L-J 2007 *J. Phys. Chem.* **C111** 16109
9. Kolb D M 1978 In *Advances in electrochemistry and electrochemical engineering* (eds) H Gerischer and C W Tobias (New York: Wiley) vol. 11, p. 127
10. Budevski E, Staikov G and Lorenz W J 1996 *Electrochemical phase formation and growth* (Weinheim: VCH)
11. Vereecken P M, Binstead R A, Deligianni H and Andricacos P C 2005 *IBM J. Res. Dev.* **49** 3
12. Staikov G (ed.) 2008 *Electrocrystallization and nanotechnology* (Weinheim: Wiley-VCH)
13. Schneeweiss M and Kolb D 1999 *Phys. Stat. Sol.* **A173** 51
14. Kolb D 2000 *Electrochim. Acta* **45** 2387
15. Herrero E, Buller L J and Abruña H D 2001 *Chem. Rev.* **101** 1897
16. Wandlowski T 2002 in *Encyclopedia of electrochemistry* (eds) M Urbakh and M Gileadi (Weinheim: Wiley-VCH) vol. 1, p. 383
17. Schultze J W and Dickertmann D 1976 *Surf. Sci.* **54** 489
18. Omar I H, Pauling H J and Juttner K J 1993 *Electrochem. Soc.* **140** 2187
19. Shi Z and Lipkowski J 1994 *J. Electroanal. Chem.* **364** 289
20. Shi Z and Lipkowski J 1994 *J. Electroanal. Chem.* **365** 303
21. Hölzle M H, Retter U and Kolb D M 1994 *J. Electroanal. Chem.* **371** 101
22. Shi Z, Wu S and Lipkowski J 1995 *Electrochim. Acta* **40** 9
23. Hölzle M H, Zwing V and Kolb D M 1995 *Electrochim. Acta* **40** 1237
24. Wu S, Lipkowski J, Tyliszczak T and Hitchcock A P 1995 *Prog. Surf. Sci.* **50** 227
25. Palomar-Pardavé M, González I and Batina N J 2000 *Phys. Chem.* **B104** 3545
26. Ataka K, Nishina G, Cai W-B, Sun S-G and Osawa M 2000 *Electrochem. Commun.* **2** 417
27. Danilov A, Molodkina E, Rudnev A, Polukarov Y M and Feliu J 2005 *Electrochim. Acta* **50** 5032
28. Borges G L, Kanazawa K K, Gordon J G II, Ashley K and Richer J 1994 *J. Electroanal. Chem.* **364** 281
29. Gordon J G, Melroy O R and Toney M F 1995 *Electrochim. Acta* **40** 3
30. Watanabe M, Uchida H, Miura M and Ikeda N 1995 *J. Electroanal. Chem.* **384** 191
31. Uchida H, Ikeda N and Watanabe M 1997 *J. Electroanal. Chem.* **424** 5
32. Uchida H, Hiei M and Watanabe M 1998 *J. Electroanal. Chem.* **452** 97
33. Nakai Y, Zei M S, Kolb D M and Lehmpfuhl G 1984 *Ber. Bunsenges. Phys. Chem.* **88** 340
34. Zei M S, Qiao G, Lehmpfuhl G and Kolb D M 1987 *Ber. Bunsenges. Phys. Chem.* **91** 349
35. Blum L, Abruña H D, White J, Gordon J G II, Borges G L, Samant M G and Melroy O R 1986 *J. Chem. Phys.* **85** 6732
36. Melroy O R, Samant M G, Borges G L, Gordon J G II, White J H, Albarelli M J, McMillan M and Abruña H D 1988 *Langmuir* **4** 728
37. Tadjeddine A, Guay D, Ladouceur M and Tourillon G 1991 *Phys. Rev. Lett.* **66** 2235
38. Toney M F, Howard J N, Richer J, Borges G L, Gordon J G II and Melroy O R 1995 *Phys. Rev. Lett.* **75** 4472
39. Nakamura M, Endo O, Ohta T, Ito M and Yoda Y 2002 *Surf. Sci.* **514** 227
40. Nakamura M, Matsunaga K, Kitahara K, Ito M and Sakata O 2003 *J. Electroanal. Chem.* **554–555** 175
41. Parry D B, Samant M G, Seki H, Philpott M R and Ashley K 1993 *Langmuir* **9** 1878
42. Futamata M 2001 *Chem. Phys. Lett.* **333** 337
43. Ito M and Nakamura M 2002 *Faraday Discuss.* **121** 71
44. Zhang J, Sung Y-E, Rikvold P A and Wieckowski A 1996 *J. Chem. Phys.* **104** 5699
45. Magnussen O M, Hotlos J, Nichols R J, Kolb D M and Behm R J 1990 *Phys. Rev. Lett.* **64** 2929
46. Magnussen O M, Hotlos J, Beitel G, Kolb D M and Behm R J 1991 *J. Vac. Sci. Technol.* **B9** 969
47. Hachiya T, Honbo H and Itaya K 1991 *J. Electroanal. Chem.* **315** 275
48. Haiss W, Lackey D, Sass J K, Meyer H and Nichols R J 1992 *Chem. Phys. Lett.* **200** 343
49. Batina N, Will T and Kolb D M 1992 *Faraday Discuss.* **94** 93
50. Will T, Dietterle M and Kolb D M 1995 In *Nanoscale probes of solid/liquid interfaces* (eds) A A Gewirth and H Siegenthaler (Kluwer, Dordrecht: NATO ASI) Series E, **288** 137
51. Xia X H, Nagle L, Schuster R, Magnussen O M and Behm R J 2000 *Phys. Chem. Chem. Phys.* **2** 4387
52. Nagy G and Wandlowski T 2003 *Z. Phys. Chem.* **217** 587
53. Nagy G and Wandlowski T 2003 *Langmuir* **19** 10271
54. Vasiljevic N, Viyannalage L T, Dimitrov N and Sieradzki K 2008 *J. Electroanal. Chem.* **613** 118
55. Manne S, Hansma P K, Massie J, Elings V B and Gewirth A A 1991 *Science* **251** 183

56. Ikemiya N, Miyaoka S and Hara S. 1994 *Surf. Sci.* **311** L641
57. Legault M, Blum L and Huckaby D A 1996 *J. Electroanal. Chem.* **409** 79
58. Rikvold P A, Zhang J, Sung Y E and Wieckowski A 1996 *Electrochim. Acta* **41** 2175
59. Brown G, Rikvold P A, Novotny M A and Wieckowski A 1999 *J. Electrochem. Soc.* **146** 1035
60. Sánchez C and Leiva E P M 1999 *Electrochim. Acta* **45** 691
61. Medved' I and Huckaby D A 2003 *J. Chem. Phys.* **118** 11147
62. Sudha V and Sangaranarayanan M V 2005 *J. Chem. Sci.* **117** 207
63. Medved' I 2008 *J. Chem. Phys.* **129** 124701
64. Shi Z, Wu S and Lipkowski J 1995 *J. Electroanal. Chem.* **384** 171
65. Wu S, Shi Z, Lipkowski J, Hitchcock A P and Tyliszczak T 1997 *J. Phys. Chem.* **B101** 10310
66. Krznarić D and Goričnik T 2001 *Langmuir* **17** 4347
67. Michaelis R 1991 Ph D thesis, Freie Universität, Berlin
68. Matsumoto H, Oda I, Inukai J and Ito M 1993 *J. Electroanal. Chem.* **356** 275
69. Matsumoto H, Inukai J and Ito M 1994 *J. Electroanal. Chem.* **379** 223
70. Hotlos J, Magnussen O M and Behm R J 1995 *Surf. Sci.* **335** 129
71. Retter U 1978 *J. Electroanal. Chem.* **87** 181